MOLECULAR AND CELLULAR BIOLOGY, Aug. 2004, p. 6799–6810 Vol. 24, No. 15
0270-7306/04/$08.00+0 DOI: 10.1128/MCB.24.15.6799–6810.2004


# Three Separable Domains Regulate GTP-Dependent Association of H-ras with the Plasma Membrane

Barak Rotblat,[1] Ian A. Prior,[2] Cornelia Muncke,[3] Robert G. Parton,[3,4] Yoel Kloog,[1] Yoav I. Henis,[1]* and John F. Hancock[3]*

*Department of Neurobiochemistry, George S. Wise Faculty of Life Sciences, Tel Aviv University, Tel Aviv, Israel[1]; The Physiological Laboratory, University of Liverpool, Liverpool, England[2]; and Institute for Molecular Bioscience[3] and Centre for Microscopy and Microanalysis and School of Biomedical Sciences,[4] University of Queensland, Brisbane, Australia*

Received 8 April 2004/Accepted 10 May 2004

**The microlocalization of Ras proteins to different microdomains of the plasma membrane is critical for signaling specificity. Here we examine the complex membrane interactions of H-ras with a combination of FRAP on live cells to measure membrane affinity and electron microscopy of intact plasma membrane sheets to spatially map microdomains. We show that three separable forces operate on H-ras at the plasma membrane. The lipid anchor, comprising a processed CAAX motif and two palmitic acid residues, generates one attractive force that provides a high-affinity interaction with lipid rafts. The adjacent hypervariable linker domain provides a second attractive force but for nonraft plasma membrane microdomains. Operating against the attractive interaction of the lipid anchor for lipid rafts is a repulsive force generated by the N-terminal catalytic domain that increases when H-ras is GTP loaded. These observations lead directly to a novel mechanism that explains how H-ras lateral segregation is regulated by activation state: GTP loading decreases H-ras affinity for lipid rafts and allows the hypervariable linker domain to target to nonraft microdomains, the primary site of H-ras signaling.**

The spatial organization of signaling proteins on the plasma membrane contributes to the regulation and coordination of signaling networks. The mechanisms whereby proteins and lipids are sequestered into specific microdomains are incompletely understood. The proposal that cholesterol-rich lipid rafts, which have been clearly demonstrated in artificial membranes, also exist and operate in biological membranes has gained widespread but not general acceptance (12, 25). There is good evidence from single-molecule tracking, fluorescence resonance energy transfer (FRET), and photonic force microscopy for cholesterol- and actin-dependent microcompartmentalization of the outer leaflet of the plasma membrane (3, 6, 16, 22, 28), although the biophysical basis of this process continues to be debated (1, 3, 12, 23, 25).

Studying the inner leaflet of the plasma membrane is even more problematic. Classical fractionation protocols that rely on detergent insolubility and flotation with light membranes on density gradients suggest that a subset of inner plasma membrane proteins associate with lipid rafts but cannot offer any insight into the spatial organization of inner leaflet proteins in intact cells. FRET studies with monomeric yellow and cyan fluorescent proteins tethered by a Fyn membrane anchor strongly suggest that lipid rafts exist on the inner plasma membrane, since FRET is abolished when cell surface cholesterol is acutely depleted (29). The putative size of lipid rafts (<100 nm) is below the resolution of the light microscope, preventing direct visualization of discrete microdomains by confocal microscopy unless rafts are first cross-linked into larger structures (8).

To address the problem of directly visualizing inner plasma membrane microdomains we used electron microscopy (EM) to study the spatial organization of Ras signaling domains. Ras proteins are small GTPases that operate as molecular switches on the inner surface of the plasma membrane. Three isoforms of Ras, H-, N-, and K-ras, are ubiquitously expressed in mammalian cells. They interact with a common set of effector and regulatory proteins, and yet each isoform generates a distinct signal output (7). These signaling differences may reflect the ability of the different Ras membrane anchors to target to distinct membrane microdomains. The membrane anchors of H-, N-, and K-ras comprise a common C-terminal *S*-farnesyl cysteine carboxy methylester operating in concert with one or two adjacent *S*-palmitoyl cysteine residues in N- and H-ras or a polybasic domain of six lysines in K-ras (7).

Sucrose gradient fractionation and functional assays in cholesterol-depleted cells show that inactive H-ras is partially localized to lipid rafts but that constitutively activated H- and K-ras fractionate away from raft markers (17). Quantitative EM analysis of intact plasma membrane sheets shows that constitutively activated H- and K-ras occupy spatially distinct nonraft microdomains and that only inactive H-ras interacts with lipid rafts (18). An independent study (14), using fluorescence recovery after photobleaching (FRAP) on living cells, reached similar conclusions: activated H- and K-ras interact with distinct nonraft sites on the plasma membrane and only inactive H-ras has significant affinity for lipid rafts.

From our studies it has become clear that the guanine nucleotide-bound state and C-terminal sequences adjacent to the membrane anchor influence whether H-ras associates with

* Corresponding author. Mailing address for John F. Hancock: Institute for Molecular Bioscience, 306 Carmody Rd., University of Queensland, Brisbane 4072, Australia. Phone: 61 7 3346 2033. Fax: 61 7 3346 2101. E-mail: j.hancock@imb.uq.edu.au. Mailing address for Yoav I. Henis: Department of Neurobiochemistry, The George S. Wise Faculty of Life Sciences, Tel Aviv University, Tel Aviv 69978, Israel. Phone: 972-3-640-9053. Fax: 972-3-640-7643. E-mail: henis@post.tau.ac.il.

lipid rafts or nonraft microdomains (17). It remains unknown, however, how H-ras plasma membrane interactions are regulated and how different elements control its overall membrane affinity and preference for different microdomains. To tackle these questions we examined a series of H-ras C-terminal mutants, which have been well characterized in terms of biological and biochemical activity, using a combination of high-resolution EM spatial mapping and FRAP analysis of living cells. Our data show that separable, attractive forces provided by the membrane anchor and linker domain of the hypervariable region (hvr) govern the interaction of H-ras with the plasma membrane. These attractive forces however operate against a repulsive force contributed by the N-terminal catalytic domain that increases on GTP loading. The results suggest a novel mechanism for regulation of H-ras lateral segregation that may be applicable to other lipidated signaling proteins. The study also shows how data generated from EM (yielding high-resolution spatial information) and FRAP (providing dynamic information from living cells), two quantitative methods of studying membrane interactions, are mutually informative.

## MATERIALS AND METHODS

**Reagents.** Affinity-purified polyclonal anti-green fluorescent protein (GFP), monoclonal anti-Ras Y13-238 antibodies, the expression constructs GFP-tH, GFP-CTH, GFP-H-ras(wt), and GFP-H-rasG12V, and hypervariable linker region mutants of GFP-H-rasG12V (GFP-H-rasG12V-Δhvr, -Δ1, -Δ2, -Δ1ala, and -Δ2ala) have been described previously (11, 14, 17, 18). GFP-H-ras(wt)-Δhvr was constructed by recombination of GFP-H-rasG12V-Δhvr with H-ras(wt). Gold-conjugated antibodies were prepared by the tannic acid-citrate method (26). Gold antibody conjugates (2- and 4-nm particle size) were purified on 10 to 40% glycerol gradients (19).

**Electron microscopy and image analysis.** BHK cells were transfected with Lipofectamine according to the manufacturer's instructions and incubated overnight in serum-free medium. Where indicated, cells were treated with 1% methyl-β-cyclodextrin (MβCD) in serum-free medium for 60 min prior to processing. Plasma membrane sheets were prepared, fixed with 4% paraformaldehyde–0.1% glutaraldehyde, labeled as described previously (18, 19), and photographed in a JEOL-1010 EM. For spatial mapping, 725-nm$^2$ areas of digitized negatives were viewed in Adobe Photoshop 7.0. Gold particles were marked with a pencil tool the same size as the particle, and the coordinates of the marked gold particles were determined using Image J. For double-labeled areas, small gold particles were distinguished from large gold particles by setting the limits for counting in Image J to values determined by precalibrating the gold fractions (18, 19).

**Statistical analysis of EM point patterns.** We have described in detail the statistical theory and methodology to derive Ripley's K-function for a single-size gold pattern and the bivariate K-function for a double-size gold pattern (18). For this study all calculations were carried out using a series of Excel macros (18, 19) that are available on request. Confidence intervals for the bivariate K-functions were derived from 200 Monte Carlo simulations of patterns with the same number of small and large gold particles used in the experiment. Confidence intervals for the K-function were calculated from published formulas (20).

**FRAP.** COS-7 cells were maintained as described previously (4). For FRAP studies, they were plated on glass coverslips in 35-mm-diameter dishes and transfected using DEAE-dextran. At 24 h posttransfection, some samples were cholesterol depleted by a 24-h incubation with 50 μM compactin and 50 μM mevalonate in Dulbecco's modified Eagle's medium containing 10% lipoprotein-deficient serum (9, 14). This procedure reduces membrane cholesterol content by 30 to 33% (14, 24) and was used because MβCD treatment has been reported to reduce the lateral diffusion rates of some nonraft proteins (14, 24). FRAP studies were conducted 48 h posttransfection at 22°C in Hank's balanced salt solution supplemented with 20 mM HEPES, pH 7.2, as described previously (14). The monitoring argon ion laser beam (488 nm, 1.2 μW) was focused through a Zeiss Universal microscope to a Gaussian radius of 0.85 ± 0.02 μm (63× objective) or 1.36 ± 0.04 μm (40× objective). A brief pulse (6 mW for 4 to 6 ms for the 63× objective and 10 to 20 ms for the 40× objective) bleached 50 to 70% of the fluorescence in the illuminated region, with recovery monitored by the attenuated monitoring beam. The apparent characteristic fluorescence recovery time τ (the time required to attain half of the recoverable fluorescence intensity for a Gaussian bleach profile) and the mobile fraction were derived by nonlinear regression analysis, fitting to a lateral diffusion process with a single τ value (15). Statistical comparisons were carried out using Student's *t* test.

**Cell fractionation.** BHK or COS-7 cells expressing GFP-tagged proteins were subjected to hypotonic lysis, and P100 and S100 fractions were prepared from postnuclear supernatants as described previously (21). A total of 20 μg of each P100 fraction and an equal proportion of the S100 fraction were immunoblotted for GFP. Blots developed using enhanced chemiluminescence were visualized and quantified by phosphorimaging (21).

**Labeling of cells with phalloidin-TRITC.** COS-7 cells transiently expressing GFP-H-ras proteins were fixed 48 h posttransfection with 3% paraformaldehyde (30 min), permeabilized with 0.2% Triton X-100, and incubated (40 min) with 0.1 μg of phalloidin-tetramethyl rhodamine isocyanate (TRITC)/ml. The cells were washed and mounted in Prolong Antifade (Molecular Probes). Transfected cells were identified by GFP fluorescence, and the TRITC-stained F-actin in these cells was visualized using a Zeiss LSM 510 confocal microscope fitted with rhodamine filters.

## RESULTS

**Biological activities of GFP-H-ras proteins in COS-7 cells.** Jaumot et al. previously reported the biological and biochemical activity of a series of constitutively active H-rasG12V proteins with deletions or alanine substitutions in the hvr linker domain adjacent to the membrane anchor (11) (for schematic representations and nomenclature, see Fig. 1A). The plasma membrane interactions of these mutants were not examined in detail, because we had not then developed EM techniques to assign proteins to morphologically featureless plasma membrane microdomains. BHK cells and PC12 cells were used for this earlier work. The FRAP analysis reported here employs COS-7 cells; therefore, we first confirmed that the biological effects of the mutant GFP-H-rasG12V proteins in these cells are similar. As a simple readout for Ras activity we examined the disassembly of actin stress fibers (27). F-actin in COS-7 cells transiently expressing GFP-H-rasG12V proteins was stained with phalloidin-TRITC and imaged by confocal microscopy (Fig. 1B). The number of transfected cells exhibiting clear stress fibers was determined (Fig. 1C). Control cells transfected with GFP vector exhibited strong stress fibers, whereas expression of GFP-H-rasG12V resulted in a nearly complete loss of stress fibers. GFP-H-rasG12V-Δhvr, GFP-H-rasG12V-Δ1, GFP-H-rasG12V-Δ2, and H-rasG12V-Δ1ala were scored biologically inactive since their expression did not cause any significant loss of stress fibers, whereas the alanine substitution mutant H-rasG12V-Δ2ala exhibited reduced activity (Fig. 1C). These results obtained with COS-7 cells agree with the previously characterized biological activities of the GFP-Ras proteins in PC-12 and BHK cells (11).

**Localization of H-ras to nonraft microdomains requires hvr linker domain sequences.** To directly visualize and quantify the microlocalization of H-ras proteins on intact plasma membranes we used a combination of immunogold EM and spatial statistics. Intact plasma membrane sheets were prepared from BHK cells (left untreated or incubated with MβCD to deplete cholesterol) expressing GFP-H-rasG12V proteins and labeled after fixation with 4-nm-particle-size gold directly coupled to affinity-purified anti-GFP antibodies (Fig. 2). The gold patterns on multiple plasma membrane sheets were analyzed using Ripley's K-function to determine whether they were random, clustered, or dispersed. As reported previously (18) and shown here (Fig. 3A), full-length H-rasG12V is clustered on the plasma membrane: the $L(r)$-$r$ curve shows a significant

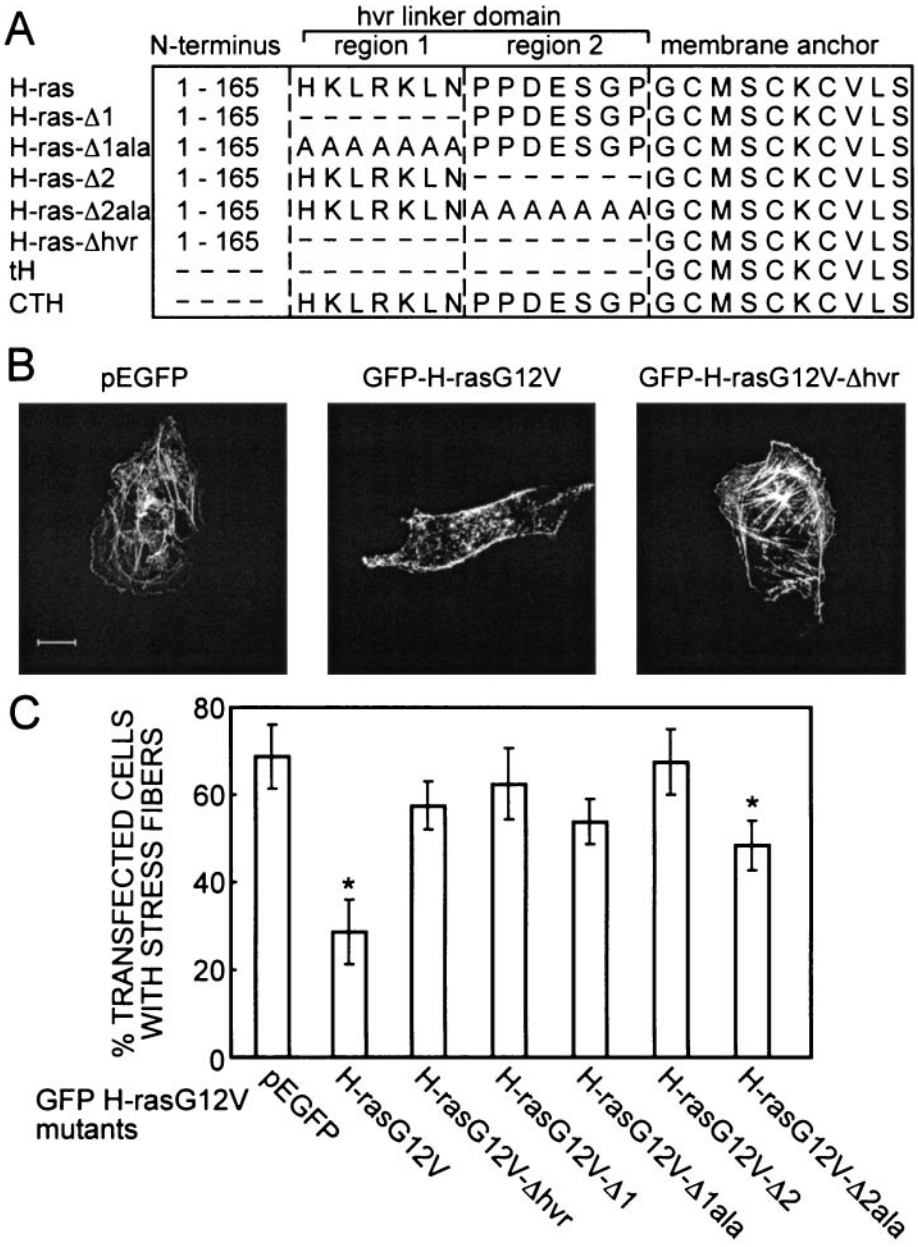


FIG. 1. Loss of biological activity of GFP-labeled H-ras hvr mutants expressed in COS-7 cells. (A) Schematics of the GFP-H-ras mutants employed. Amino acids are depicted in single-letter code. All constructs contain N-terminal EGFP. Mutants were generated on a background of constitutively active H-rasG12V or nonactivated H-ras(wt). (B) Examples of the effect of H-rasG12V expression on actin stress fibers. Transiently transfected COS-7 cells were labeled with phalloidin-TRITC. Cells expressing GFP (vector control) or GFP-H-rasG12V-Δhvr, but not GFP-H-rasG12V, show strong labeling of stress fibers. Bar, 10 μm. (C) Graph showing the fraction of transfected (GFP-expressing) cells that exhibit clear stress fibers, expressed as means ± standard deviations ($n = 80$ in each bar). Significant reductions (identified by $t$ tests) in the mean values compared to those of cells transfected with GFP alone are indicated (*): $P < 0.01$ for H-rasG12V, $P < 0.02$ for H-rasG12V-Δ2ala.

positive deviation out of the 99% confidence interval for complete spatial randomness (CSR) at a radius of 20 nm (Fig. 3A). The clustering of H-rasG12V is unaffected by cholesterol depletion, indicating association with cholesterol-independent microdomains (Fig. 3) (18). Figure 3B shows that deletion of the complete hvr linker domain (amino acids 166 to 180: H-rasG12V-Δhvr) has a fundamental effect on the microlocalization of H-ras: H-rasG12V-Δhvr is clustered, as indicated by the substantial positive deflection of the $L(r)$-$r$ curve outside the 99% CSR confidence interval, but clustering is completely abolished in MβCD-treated cells. We conclude that H-rasG12V-Δhvr is localized to lipid rafts. Raft localization is also evident for H-rasG12V-Δ1, H-rasG12V-Δ1ala, and H-rasG12V-Δ2 (Fig. 3C to E; for structure, see Fig. 1A), which are significantly clustered, but their clustering is substantially reduced upon cholesterol depletion. Unlike H-rasG12V-Δhvr, however, H-rasG12V-Δ1, H-rasG12V-Δ1ala, and H-rasG12V-Δ2 must retain some affinity for nonraft microdomains, because the $L(r)$-$r$

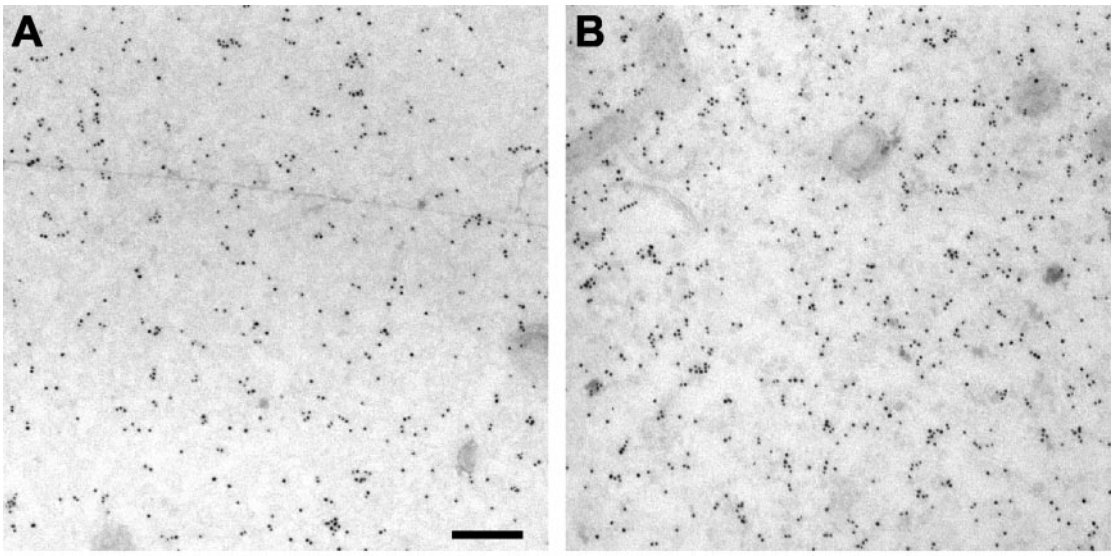


FIG. 2. Immunogold labeling of Ras proteins on plasma membrane sheets. Examples of plasma membrane sheets from BHK cells expressing GFP-H-rasG12V and labeled with 4-nm-particle-size gold conjugated directly to affinity-purified polyclonal anti-GFP antibody are shown. (A) Untreated cells. (B) Cells treated for 60 min with 1% MβCD before the sheets were prepared. Bar, 100 nm.

curves do not fall completely into the CSR envelope. This indicates residual clustering after lipid raft disassembly with MβCD (Fig. 3C to E). The microlocalization of H-rasG12V-Δ2ala closely resembles that of full-length H-rasG12V and exhibits the same degree of clustering irrespective of whether cell surface cholesterol is depleted (Fig. 3F).

To confirm the assignment of H-rasG12V-Δ1, H-rasG12V-Δ1ala, and H-rasG12V-Δ2 but not H-rasG12V-Δ2ala to lipid rafts, they were coexpressed in BHK cells with the lipid raft marker GFP-tH (schematically shown in Fig. 1A). Plasma membrane sheets from transfected cells were colabeled with 4-nm-particle-size gold conjugated to anti-GFP and 2-nm-particle-size gold conjugated to anti-Ras (Y13-238). The extent of colocalization of Ras mutants with GFP-tH was then quantified using bivariate K-functions to analyze the gold patterns (Fig. 4). The null hypothesis for bivariate analysis is that the gold particle populations are randomly arrayed around each other; thus, positive deflections of an $L_{biv}(r)$-$r$ curve above the 95% confidence interval indicate significant colocalization of the two sets of gold particles. By these criteria, H-rasG12V-Δ1, H-rasG12V-Δ1ala, and H-rasG12V-Δ2 colocalize with the raft marker GFP-tH whereas H-rasG12V-Δ2ala does not (Fig. 4).

These data suggest that hvr linker sequences are required for the interaction of H-ras with nonraft microdomains. To confirm this, we investigated whether these sequences are sufficient to alter the targeting of GFP-tH to lipid rafts. To this end we studied the microlocalization of GFP-CTH, which contains the entire H-ras hvr (amino acids 166 to 189) fused to GFP rather than just the minimal membrane anchor present in GFP-tH (Fig. 1A). In contrast to GFP-tH, which is exclusively clustered in cholesterol-dependent lipid rafts (18) (Fig. 5), GFP-CTH also clusters outside lipid rafts, as evidenced by its persistent clustering in cholesterol-depleted cells (Fig. 5). Finally, to complete the EM analysis, we show that GFP-H-ras(wt)-Δhvr clusters in lipid rafts, as demonstrated by the loss of its clustering upon cholesterol depletion (Fig. 5).

**Distinct roles for H-ras anchor and hvr linker domains in regulating membrane association.** EM provides high-resolution spatial information but is restricted to fixed membrane sheets. To probe the dynamics of Ras-membrane interactions in living cells we used FRAP. We first compared the fluorescence recovery of GFP-H-rasG12V and GFP-H-rasG12V-Δhvr. Typical FRAP curves are shown in Fig. 6, and the averaged results are depicted in Fig. 7. GFP-H-rasG12V had a characteristic fluorescence recovery time $\tau$ (2) of ~0.4 s with a laser beam with a Gaussian radius of 0.85 μm, in keeping with our previously reported lateral diffusion coefficient ($D$) of $\sim 5 \times 10^{-9}$ cm$^2$/s (Fig. 6A) (14). Interestingly, the fluorescence recovery of GFP-H-rasG12V-Δhvr was much faster ($\tau \sim 0.1$ s; Fig. 6B), although it was still more than an order of magnitude slower than that of free GFP in the cytosol, which recovered at a rate faster than the experimental time scale ($\tau < 0.005$ s; Fig. 6C). This indicates that the fluorescence recovery of GFP-H-rasG12V is retarded relative to that of GFP-H-rasG12V-Δhvr.

To further investigate this difference we performed FRAP with laser beams of different sizes (5, 10, 13). If FRAP occurs by lateral diffusion, $\tau$ is essentially the characteristic diffusion time $\tau_D$ and is proportional to the area illuminated by the beam ($\tau_D = \omega^2/4D$, where $\omega$ is the Gaussian radius of the laser beam). When FRAP takes place by dynamic exchange between membrane-bound and cytosolic pools (as may occur for weaker, transient interactions with the membrane), $\tau$ reflects the chemical relaxation time due to exchange, which is equal on all surface regions regardless of whether they are illuminated by the beam, and therefore does not depend on the beam size (5, 10, 13). The expected ratio of $\tau(40\times)/\tau(63\times)$ for the two beam sizes generated using the 40× and 63× objectives, respectively, is 2.56 for pure lateral diffusion or 1 (no dependence on beam size) for pure exchange (see legend to Fig. 7) (10). In agreement with earlier results (13), GFP-H-rasG12V exhibited pure lateral diffusion, as evident by a

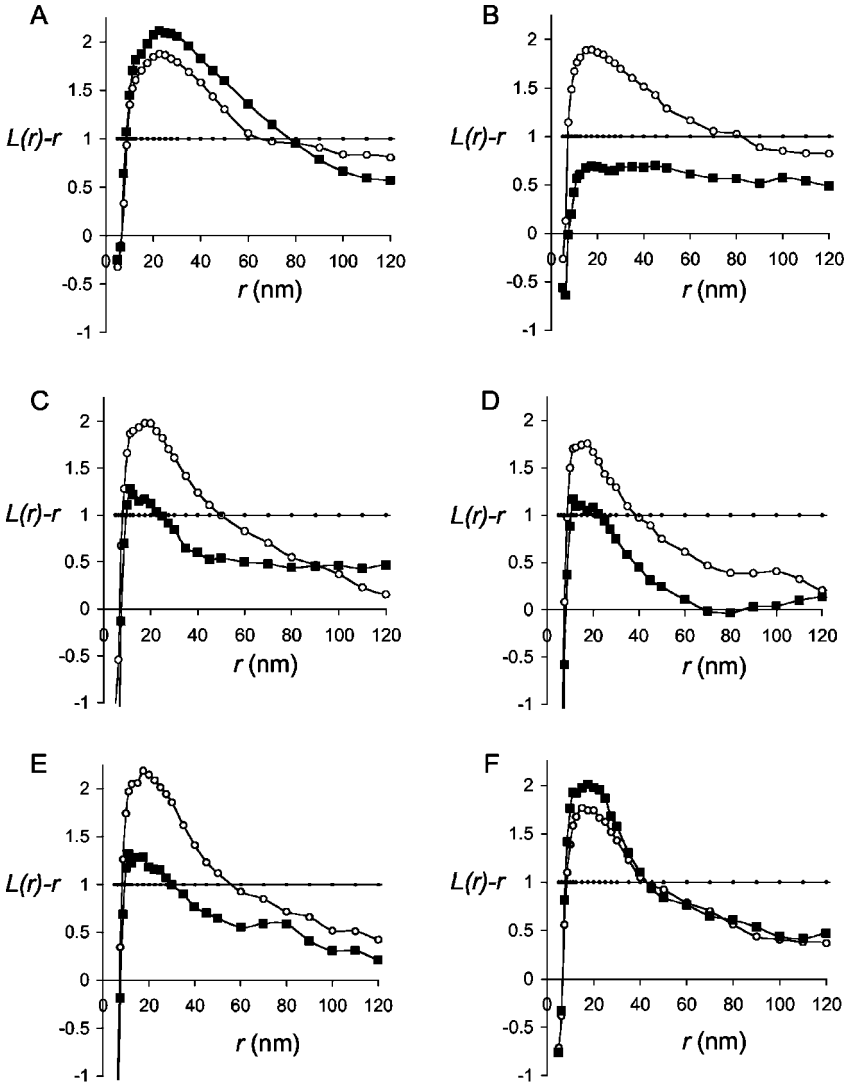


FIG. 3. Spatial mapping of H-ras proteins by univariate K-functions. Plasma membrane sheets were prepared from BHK cells transiently expressing GFP-tagged H-rasG12V (A), H-rasG12V-Δhvr (B), H-rasG12V-Δ1 (C), H-rasG12V-Δ1ala (D), H-rasG12V-Δ2 (E), or H-rasG12V-Δ2ala (F) and were treated for 60 min with 1% MβCD (■) or left untreated (○). Sheets were labeled with 4-nm-particle-size gold conjugated directly to affinity-purified polyclonal anti-GFP antibody, and the gold patterns in areas 725 by 725 nm in size were analyzed using spatial statistics. The graphs show mean univariate K-functions expressed as $L(r)$-$r$ standardized on the 99% confidence interval for CSR (●). Each curve represents data pooled from multiple ($n$ = 6 to 12) plasma membrane sheets. The average labeling density was 584 gold particles/$\mu m^2$.

$\tau(40\times)/\tau(63\times)$ ratio of 2.4 that is not significantly different from the experimentally determined ratio between the areas illuminated by the laser beam with the two objectives ($P > 0.1$; Fig. 7A). In contrast, the fluorescence of GFP-H-rasG12V-Δhvr recovered by pure exchange, as evident from the $\tau(40\times)/\tau(63\times)$ ratio of 0.9 that is not significantly different from the value of 1.0 expected for pure exchange ($P > 0.1$; Fig. 7A). Since GFP-H-rasG12V and GFP-H-rasG12V-Δhvr are expressed at similar levels of density on the plasma membrane (Fig. 3), these FRAP data suggest that GFP-H-rasG12V-Δhvr has a weaker interaction with the membrane (transient versus stable) than GFP-H-rasG12V. Thus, the hvr linker domain contributes not only to the lateral segregation of GFP-H-rasG12V into nonraft microdomains (10) (Fig. 2) but also to the overall strength of interactions with the plasma membrane.

**The N-terminal catalytic domain of H-ras weakens plasma membrane interactions.** The conclusion that the hvr linker domain is essential for stable membrane association of GFP-H-rasG12V suggested that the lipid-modified anchor by itself might not be sufficient for stable membrane binding. To examine this possibility we investigated the membrane interactions of GFP targeted to the plasma membrane by the minimal C-terminal anchor of H-ras (GFP-tH). GFP-tH exhibited stable membrane association and pure lateral diffusion, as evident by its $\tau(40\times)$ and $\tau(63\times)$ values and ratio, which were similar to those of GFP-H-rasG12V ($P > 0.1$ in all cases; Fig. 7A). Thus, out of the context of full-length H-rasG12V, the H-ras minimal anchor is sufficient for stable membrane association. However, when this anchor is connected to the N-terminal domains of H-ras, omission of the hvr linker (GFP-H-

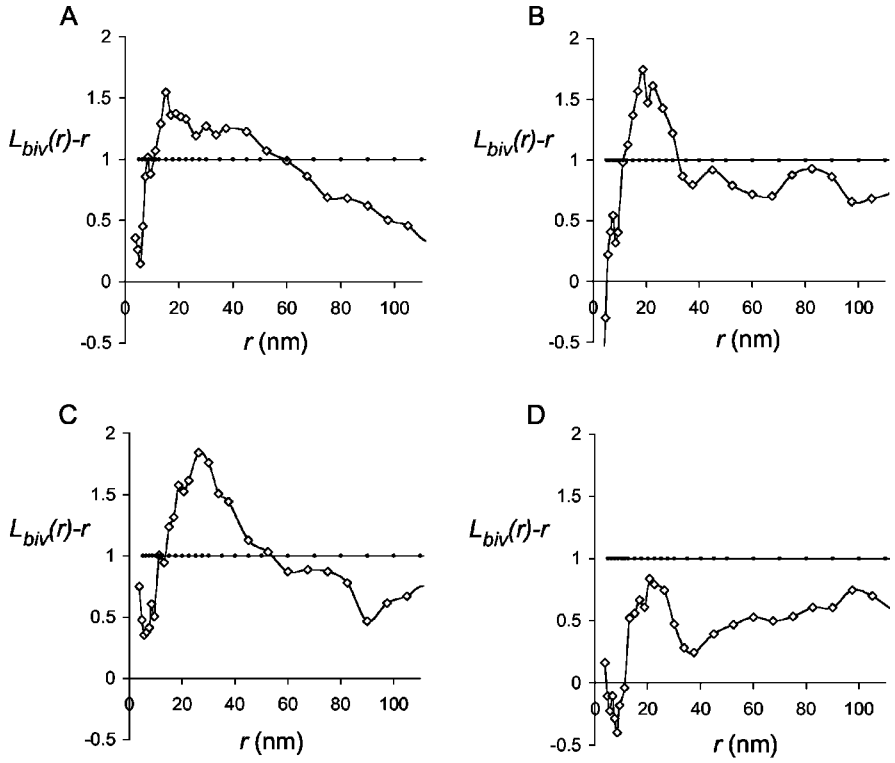


FIG. 4. Spatial mapping of H-ras proteins to lipid rafts using bivariate K-functions. Plasma membrane sheets were prepared from BHK cells coexpressing GFP-tH and (untagged) H-rasG12V-Δ1 (A), H-rasG12V-Δ1ala (B), H-rasG12V-Δ2 (C), or H-rasG12V-Δ2ala (D). Sheets were colabeled with monoclonal antisera to Ras (Y13-238) coupled directly to 4-nm-particle-size gold and anti-GFP antisera coupled directly to 2-nm-particle-size gold. Coclustering of the 2- and 4-nm-particle-size gold in study areas 725 by 725 nm in size was analyzed by spatial statistics. The graphs show mean bivariate K-functions expressed as $L_{biv}(r)$-$r$ standardized on the 95% confidence interval for CSR (●). Each curve represents data pooled from multiple ($n$ = 6 to 9) plasma membrane sheets. The average labeling density was 26 (4 nm) and 145 (2 nm) gold particles/$\mu m^2$.

rasG12V-Δhvr) results in exchange (Fig. 7A). Taken together, these data strongly suggest that the catalytic N-terminal domains of GFP-H-rasG12V generate a repulsive force that weakens the association of H-ras with the membrane.

The N-terminal catalytic domain of Ras proteins undergoes marked conformational changes between the GDP- and GTP-bound states. We therefore examined whether GTP loading might regulate the repulsive force exerted by the N-terminal region on H-ras membrane binding. We reasoned that any differences would be more marked in H-ras proteins that lack the hvr linker domain and are solely dependent on the anchor for membrane association. In contrast to GTP-bound GFP-H-rasG12V-Δhvr that recovers solely by exchange, GDP-bound GFP-H-ras(wt)-Δhvr exhibits a mixed mode of fluorescence recovery (i.e., a contribution from both lateral diffusion and exchange), as indicated by the $\tau(40\times)/\tau(63\times)$ ratio (1.6), which is significantly different from both 1 and 2.56 ($P < 0.001$ in both cases) (Fig. 7A). This suggests that GTP-loaded GFP-H-rasG12V-Δhvr has a weaker membrane interaction than GDP-loaded GFP-H-ras(wt)-Δhvr, a conclusion also supported by the higher $\tau$ values measured for GFP-H-ras(wt)-Δhvr with both beam sizes. Together, the data show that of the GDP- and GTP-bound states of the Δhvr mutants, the former has the stronger and more stable interaction with the membrane, although this interaction is not as strong as that of the stably interacting (i.e., laterally diffusing) full-length GFP-H-ras(wt) (Fig. 7A). We conclude that the conformation of the catalytic N-terminal domain regulates H-ras membrane interactions, with GTP binding to H-ras increasing the repulsive force. Thus, H-ras exhibits GTP-dependent regulation of membrane affinity.

A testable prediction of this conclusion is that there may be a greater cytosolic pool of GFP-H-rasG12V-Δhvr than GFP-H-ras(wt)-Δhvr. BHK cells expressing GFP-H-rasG12V-Δhvr, GFP-H-ras(wt)-Δhvr, and a range of control proteins were therefore fractionated into S100 and P100 fractions and quantitatively immunoblotted for GFP (Fig. 8). The fraction of GFP-H-rasG12V-Δhvr and GFP-H-ras(wt)-Δhvr stably associated with cell membrane was significantly reduced ($P < 0.001$ in both cases) compared to that full-length GFP-H-rasG12V. Significantly ($P < 0.001$) more GFP-H-ras(wt)-Δhvr was membrane associated than GFP-H-rasG12V-Δhvr, in full consistency with the FRAP data. Similar results (data not shown) were obtained with COS-7 cells. Interestingly, a significant ($P < 0.05$) difference was also measurable between GFP-tH and GFP-CTH, a result consistent with GFP-CTH having a greater membrane affinity than GFP-tH (Fig. 8).

**The hvr linker domain is required for stable binding to nonraft microdomains.** To examine whether the anchor and linker hvr domains of H-ras interact predominantly with raft or nonraft microdomains, we studied by FRAP the effects of cholesterol depletion on the membrane affinity of GFP-H-ras. In accord with former studies (14), both GFP-H-rasG12V and GFP-H-ras(wt) exhibited fluorescence recovery by pure lateral

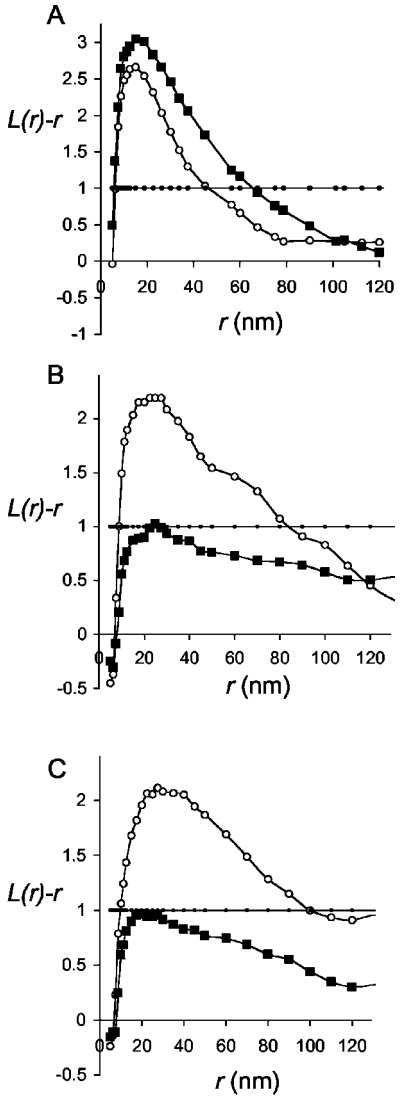


FIG. 5. The hvr linker domain modulates H-ras interactions with raft and nonraft microdomains. Plasma membrane sheets were prepared from BHK cells transiently expressing GFP-CTH (A), GFP-tH (B), or GFP-H-ras(wt)-Δhvr (C) and treated for 60 min with 1% MβCD (■) or left untreated (○). Sheets were labeled with 4-nm-particle-size gold coupled directly to affinity-purified polyclonal anti-GFP antibody, and the gold patterns in study areas 725 by 725 nm in size were analyzed by spatial statistics. The graphs show mean univariate K-functions expressed as $L(r)$-$r$ standardized on the 99% confidence interval for CSR (●). Each curve represents data pooled from multiple ($n$ = 6 to 12) plasma membrane sheets. The average labeling density was 225 gold particles/$\mu m^2$.

diffusion [$\tau(40\times)/\tau(63\times)$ not significantly different from 2.56; $P > 0.2$] after cholesterol depletion (Fig. 7B). However, the effects of cholesterol depletion on the lateral diffusion rates were much more pronounced for GFP-H-ras(wt), in accord with its partial localization to lipid rafts (17, 18). Thus, neither clustering of GFP-H-rasG12V (Fig. 2) nor its continuous membrane association (Fig. 7) requires lipid rafts. In contrast, cholesterol depletion had a strong impact on $\tau$ of GFP-H-rasG12V-Δhvr, which became too fast to be measured at our time scale ($\tau < 0.005$ s, in similarity to GFP results; Fig. 7B). This indicates that the normally raft-resident GFP-H-rasG12V-Δhvr is very loosely associated with the membrane in the absence of rafts, in keeping with its random membrane distribution following cholesterol depletion (Fig. 3). This could be a result of strong manifestation of the repulsive forces from the N-terminal domain and/or a loss of positive attractive forces from the lipid-modified anchor.

To distinguish between these two possibilities, we performed FRAP studies on cholesterol-depleted cells expressing GFP-tH and GFP-CTH. The $\tau$ values of GFP-tH, which has only the lipid anchor, decreased significantly (1.3-fold; $P < 0.001$) following cholesterol depletion (Fig. 7), indicating a reduction in interaction with the membrane. However, this reduction was

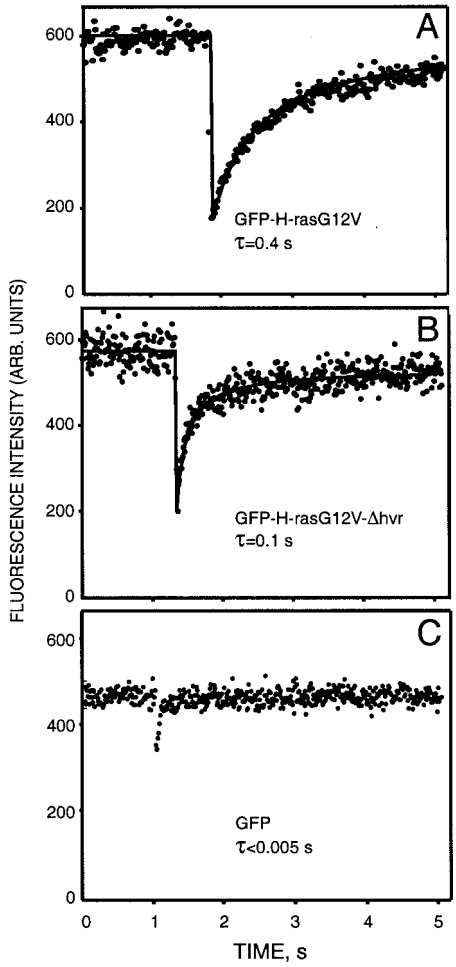


FIG. 6. The fluorescence recovery rate of GFP-H-rasG12V is retarded relative to that of GFP-H-rasG12V-Δhvr. FRAP experiments (with a 63× lens objective) were conducted with COS-7 cells transiently expressing GFP-H-rasG12V (A), GFP-H-rasG12V-Δhvr (B), or GFP (C). The dots represent the fluorescence intensities. Solid lines show the best fit of a nonlinear regression analysis. GFP (C) exhibits free diffusion in the cytoplasm, resulting in extremely fast fluorescence recovery. Thus, free diffusion in the cytoplasm occurs on a faster time scale and does not contribute significantly to the measurements depicted in panels A and B. Fluorescence recovery rates of GFP-H-rasG12V and GFP-H-rasG12V-Δhvr are significantly slower than that of free GFP, enabling accurate determination of the characteristic fluorescence recovery time $\tau$. The mobile fractions were high (~96%) in all cases.

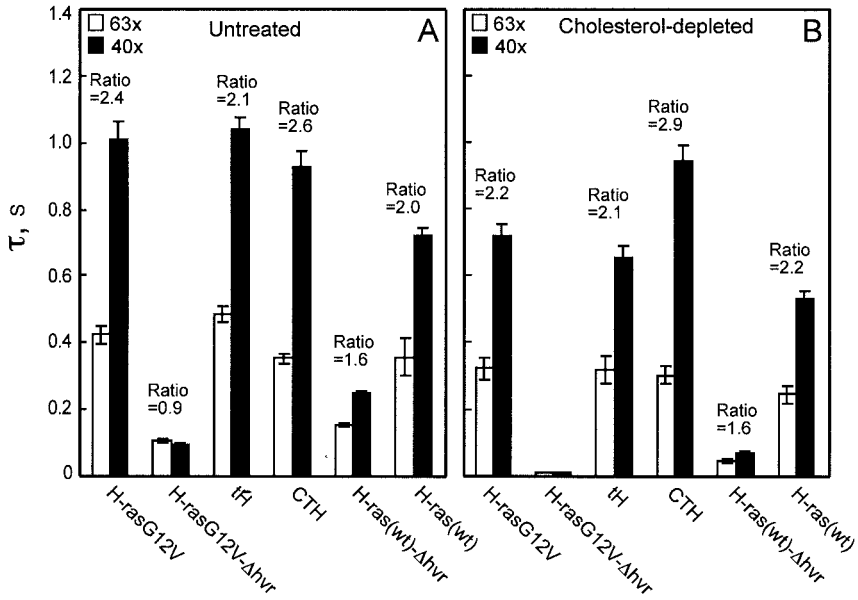


FIG. 7. Determination by FRAP of the contribution of the lipid anchor, hvr linker, and N-terminal domains to H-ras membrane interactions. FRAP experiments were conducted on COS-7 cells transiently expressing GFP-H-rasG12V, GFP-H-rasG12V-Δhvr, GFP-tH, GFP-CTH, GFP-H-ras(wt)-Δhvr, and GFP-H-ras(wt). Cells were left untreated (A) or subjected to cholesterol depletion (B) prior to assay. Each bar represents the mean ± standard error of the mean (SEM) of 40 to 60 measurements. The mobile fractions were high (>90%) for all proteins. Two beam sizes were generated using 63× and 40× objectives. The fluorescence recovery times ($\tau$) were determined with each objective, and the $\tau(40\times)/\tau(63\times)$ ratios were derived. We used *t* tests to determine whether the ratios differed significantly from that expected for pure lateral diffusion: an experimentally determined ratio between the areas illuminated by the laser beam using the two objectives (mean ± SEM value of 2.56 ± 0.30; $n = 39$). Most GFP-H-ras proteins displayed $\tau$ ratios between 2.56 and 1 in both untreated and cholesterol-depleted cells, indicative of a mixture of lateral diffusion and exchange. GFP-H-rasG12V-Δhvr had similar $\tau(40\times)$ and $\tau(63\times)$ values close to the theoretical ratio of 1 expected for pure exchange (for *P* values, see text). For those GFP-H-ras proteins that display fluorescence recovery by pure (or nearly pure) lateral diffusion, it is possible to interpret the $\tau$ values into lateral diffusion coefficients. Averaging the $\tau$ values obtained with the two beam sizes, the *D* values obtained for these mutants in untreated cells were $4.4 \times 10^{-9}$, $4.1 \times 10^{-9}$, $5.0 \times 10^{-9}$, and $5.2 \times 10^{-9}$ cm$^2$/s for GFP-H-rasG12V, GFP-tH, GFP-CTH, and GFP-H-ras(wt), respectively. In cholesterol-depleted cells, the *D* values were $5.9 \times 10^{-9}$, $6.3 \times 10^{-9}$, $5.2 \times 10^{-9}$, and $7.9 \times 10^{-9}$ cm$^2$/s for the same mutants, respectively.

insufficient to shift the fluorescence recovery to exchange (Fig. 7B). This suggests that without the repulsive force exerted by the N-terminal domain, the minimal lipid anchor can still interact with the membrane in cholesterol-depleted cells and that the N-terminal domain is primarily responsible for the loss of membrane affinity of GFP-H-rasG12V-Δhvr in the absence of rafts. GFP-CTH, which possesses both the lipid anchor and the hvr linker domains of H-ras (Fig. 1A), exhibited, as expected, stable membrane interaction in untreated cells with a $\tau(40\times)/\tau(63\times)$ ratio indistinguishable from that expected of pure lateral diffusion ($P > 0.2$; Fig. 7A). The positive contribution of the hvr linker domain to the membrane association of this protein is reflected in its stable membrane association even after cholesterol depletion, as indicated by the lack of change in either its $\tau$ values or $\tau(40\times)/\tau(63\times)$ ratio in the treated cells (Fig. 7B). These data suggest that the hvr linker domain contributes mainly to association with nonraft domains.

**The hvr linker domain contains two regions that contribute differently to membrane affinity.** The H-ras hvr linker domain has been tentatively divided into two regions: region 1 and region 2 (Fig. 1 and 9) (11). Given our data showing that the hvr linker contributes to H-ras membrane interactions (Fig. 3, 4, and 7), we evaluated by FRAP the specific contribution of regions 1 and 2 by the use of H-ras mutants in which the regions were lacking or replaced with alanines (Fig. 9). A comparison of GFP-H-rasG12V-Δ1 (missing region 1) and GFP-H-rasG12V-Δ1ala (region 1 sequence replaced by alanines; Fig. 1A and 9) showed that both proteins exhibited fluorescence recovery by pure lateral diffusion [$\tau(40\times)/\tau(63\times)$ ratio, 2.0 to 2.3; Fig. 9A]. These values are very close to that of full-length H-rasG12V and suggest stable associations with the membrane. Cholesterol depletion significantly weakened these interactions but did not eliminate them altogether (Fig. 9B), as illustrated by the smaller $\tau$ values and the shift of the fluorescence recovery to exchange [$\tau(40\times)/\tau(63\times)$ ratio of 0.9, not significantly different from 1; $P > 0.2$]. We conclude that region 2 of the hvr linker, present in both mutants, contributes to the interactions of H-rasG12V with the membrane. In addition, the interactions of H-rasG12V-Δ1ala and H-rasG12V-Δ1 appear to be with both raft and nonraft sites, in accord with the EM clustering analysis (Fig. 3C and D).

In H-ras mutants lacking region 1, the correct position of region 2 is retained immediately adjacent to the C-terminal lipid-modified anchor. However, in the mutants missing region 2 (GFP-H-rasG12V-Δ2 and GFP-H-rasG12V-Δ2ala; Fig. 1A), region 1 is retained in its original position only in the alanine substitution mutant. GFP-H-rasG12V-Δ2ala displays stable membrane interactions not significantly different from those of full-length H-rasG12V [$\tau(40\times)/\tau(63\times) = 2.3$; $P > 0.1$], and this strong interaction is insensitive to cholesterol depletion [$\tau(40\times)/\tau(63\times) = 2.5$; $P > 0.1$] (Fig. 9). On the other hand,

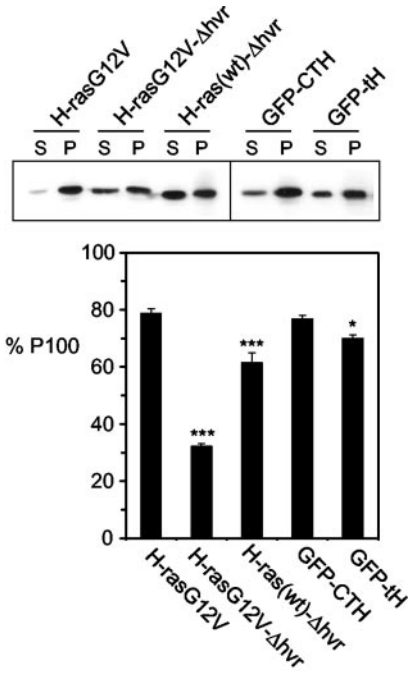


FIG. 8. Membrane affinity of H-ras proteins is reflected in the extent of P100 association. Equal proportions of cytosolic (S100) and membrane (P100) fractions prepared from BHK cells expressing GFP-tagged proteins were analyzed by quantitative immunoblotting. The fraction of GFP protein associated with the P100 was calculated as follows: P100/S100 + P100. The upper panel shows a representative immunoblot, and the graph shows data pooled from multiple experiments expressed as means ± SEMs ($n = 6$). Significant differences from GFP-H-rasG12V results identified by a Newman-Keuls multiple comparison test are indicated as * for $P < 0.05$ and *** for $P < 0.001$.

GFP-H-rasG12V-Δ2 (in which region 1 is out of the original context and is moved up to be adjacent to the lipid anchors) displays impaired membrane interactions: in untreated cells, it exhibits exchange [$\tau(40\times)/\tau(63\times) = 0.8$], and cholesterol depletion further reduces its membrane interactions, resulting in a fluorescence recovery rate faster than the experimental time scale (Fig. 9B). We conclude that region 1 of the hvr linker makes a major contribution to H-rasG12V membrane interactions but that this contribution requires region 1 to be correctly positioned in the context of the protein relative to the lipid-modified C-terminal anchor. The interaction of region 1 with the membrane appears to be with cholesterol-insensitive, non-raft sites. These results are in excellent agreement with the EM data (Fig. 3E to F and 4).

## DISCUSSION

The interaction of lipidated proteins with cell membranes is dependent on the lipid anchor. We show here, however, that for the H-ras small GTPase, plasma membrane anchoring is the product of three separable forces, of which only one is generated by the lipid anchor. The forces operating on H-ras to modulate plasma membrane attachment were revealed using a combination of FRAP to differentiate between stable and transient membrane attachment and quantitative EM to identify the spatial interactions. The minimal H-ras anchor, comprising the processed CAAX motif plus the adjacent palmitoylation sites, is sufficient to target GFP to the plasma membrane. The FRAP analysis reported here (Fig. 7) shows that GFP-tH is stably associated with the plasma membrane such that fluorescence recovery occurs exclusively by lateral diffusion. EM analysis (Fig. 4 and 5) (18) illustrates that GFP-tH is clustered in cholesterol-dependent lipid raft microdomains. Together these data show that the minimal membrane anchor of H-ras provides a high-affinity membrane interaction primarily with plasma membrane lipid rafts (see proposed model in Fig. 10). The affinity of the minimal anchor for the plasma membrane is reduced when lipid rafts are disassembled by cholesterol depletion (reflected by faster $\tau$ values) but remains sufficiently strong to prevent a shift of the FRAP to exchange (Fig. 7). In consequence, as shown by EM, there is no loss of GFP-tH from the plasma membrane in cholesterol-depleted cells but GFP-tH is no longer clustered and is randomly distributed (18).

In contrast, GFP-H-rasG12V-Δhvr, which has exactly the same membrane anchor as GFP-tH, does not interact stably with the plasma membrane. FRAP of GFP-H-rasG12V-Δhvr occurs by exchange and in cholesterol-depleted cells becomes too fast to be measured experimentally, showing severely reduced membrane affinity (Fig. 7). EM analysis (Fig. 3) shows however that GFP-H-rasG12V-Δhvr is still attached to the

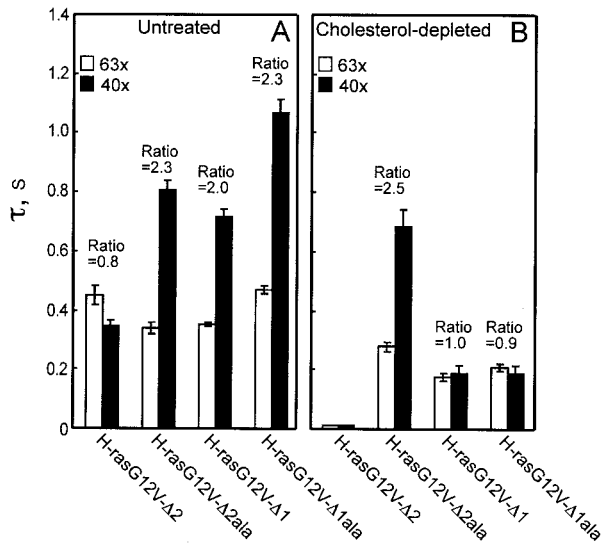


FIG. 9. FRAP analysis of the contribution of the hvr linker regions 1 and 2 to H-ras membrane affinity. FRAP experiments were conducted on COS-7 cells transiently expressing GFP-H-rasG12V-Δ2, GFP-H-rasG12V-Δ2ala, GFP-H-rasG12V-Δ1, and GFP-H-rasG12V-Δ1ala. Cells were left untreated (A) or subjected to cholesterol depletion (B). The $\tau$ values and $\tau(40\times)/\tau(63\times)$ ratios were derived as described for Fig. 7. Each bar represents the mean ± SEM of 40 to 60 measurements. The levels of the mobile fractions were high (>90%) for all GFP-Ras proteins. The significance of differences between the $\tau$ values or between the $\tau(40\times)/\tau(63\times)$ ratios measured for different mutants (or between these values measured for a specific H-ras-derived protein in untreated versus cholesterol-depleted cells) was evaluated in $t$ tests (for $P$ values, see text). For the mutants displaying recovery by pure lateral diffusion, the $D$ values were calculated from the $\tau$ values obtained with the two beam sizes. In untreated cells, the $D$ values were $5.6 \times 10^{-9}$, $5.8 \times 10^{-9}$, and $4.1 \times 10^{-9}$ cm$^2$/s for GFP-H-rasG12V-Δ2ala, GFP-H-rasG12V-Δ1, and GFP-H-rasG12V-Δ1ala, respectively. In cholesterol-depleted cells, only GFP-H-rasG12V-Δ2ala displayed recovery by lateral diffusion, with $D = 6.4 \times 10^{-9}$ cm$^2$/s.

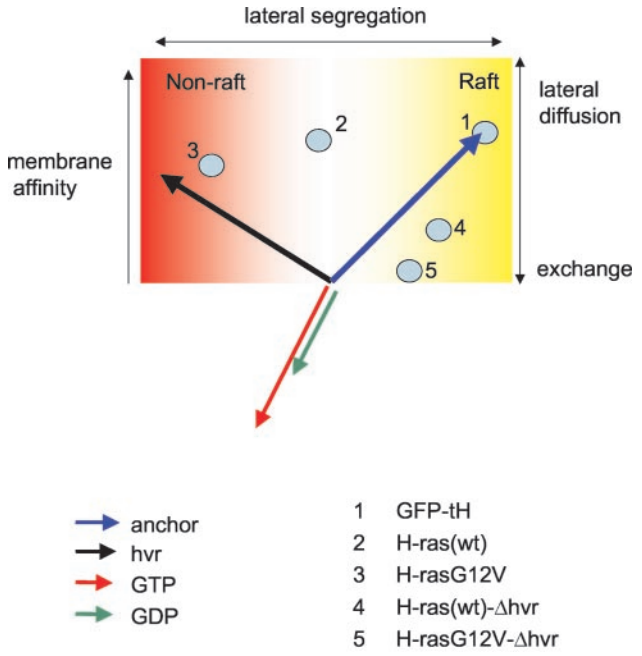


FIG. 10. A model for the interactions of H-Ras with the cell membrane. Three separable forces operate on H-ras at the plasma membrane and are represented by vectors: the direction of each vector towards raft or nonraft domains (*x* direction) is determined from the EM spatial mapping data, whereas the magnitude of attraction or repulsion from the membrane (*y* direction) is determined from the FRAP analysis. Each vector therefore integrates data derived from the two experimental approaches. Adding together all the vectors operating on a given Ras protein gives an indication of overall affinity for the membrane (*y* direction) and likelihood of segregation to raft of nonraft microdomains (*x* direction). For example, only the anchor force (blue vector) operates on GFP-tH, driving the protein into a high-affinity interaction with lipid rafts. When the N-terminal domains of Ras are present, a repulsive force (green vector) opposes the attractive force from the anchor: the repulsive force is greater still when the N terminus is GTP loaded (red vector). Adding the forces together, as in H-ras(wt)-Δhvr (blue and green vector) or H-rasG12V-Δhvr (blue and red vector), drives the proteins into low-affinity interactions that are nevertheless still predominantly with lipid rafts. In the full-length H-rasG12V an additional attractive force from the hvr (black vector) operates, shifting the low-affinity raft interaction of H-rasG12V-Δhvr into a high-affinity interaction with nonraft microdomains. The model predicts that the shift from rafts to nonraft domains is less for GDP-loaded H-ras(wt), because the repulsive force operating against the anchor force is smaller: the vector model therefore accounts for the GTP-dependent lateral segregation of H-ras. Analysis of the hvr linker mutants suggests that the single hvr vector illustrated is the sum of two vectors (data not shown) representing the relative contributions of region 1 and region 2 as discussed in the text.

plasma membrane, clustering in lipid rafts, or distributed randomly over the membrane when cells are cholesterol depleted. The simplest interpretation of the combined data is that the N-terminal catalytic domain of H-ras generates a repulsive force that opposes the affinity of the anchor for lipid rafts (Fig. 10). Interestingly, the repulsive force is reduced when H-ras is GDP loaded: FRAP of GFP-H-ras(wt)-Δhvr occurs by a combination of exchange and lateral diffusion in normal and cholesterol-depleted cells. Thus, the anchor generates a more stable membrane interaction for GDP-bound H-ras(wt)-Δhvr than for GTP-loaded GFP-H-rasG12V-Δhvr, a conclusion supported by cell fractionation results (Fig. 8). In both cases, EM shows that the anchor still targets to lipid rafts.

The membrane interactions of the lipid anchor are further modified when the hvr linker domain is present. The linker domain provides the C terminus of H-ras with a second source of membrane affinity but one that is predominantly for nonraft sites on the plasma membrane (see model in Fig. 10). Several lines of evidence support this conclusion. First, the fluorescence recovery time for GFP-CTH, which has the H-ras hvr linker domain and the lipid anchor, is unaffected by cholesterol depletion (Fig. 7). This demonstrates that there is no reduction in its membrane affinity when lipid rafts are lost. Secondly, EM shows that under the same conditions GFP-CTH remains clustered on the plasma membrane (Fig. 5). Thirdly, in contrast to GFP-H-ras(wt)-Δhvr and GFP-H-rasG12V-Δhvr, full-length GFP-H-ras(wt) and GFP-H-rasG12V, which have the hvr linker sequence, exhibit high-level affinity and stable interactions with the plasma membrane, as measured by FRAP, in the presence or absence of lipid rafts. EM identifies the site of interaction of the hvr linker as a nonraft microdomain (Fig. 3 and 5). The more extensive loss of affinity of the anchor for lipid rafts when H-ras-Δhvr is GTP loaded strongly suggests that the membrane attachment of H-ras-GTP is more dependent on the hvr than that of H-ras-GDP: given that the affinity of the hvr linker is predominantly for nonraft microdomains, these observations offer a basic mechanism for the GTP-dependent lateral segregation of H-ras out of lipid rafts that has been reported previously (Fig. 10) (17, 18).

Earlier work has suggested that the hvr linker domain can be functionally divided into two separate regions designated region 1 and region 2 (Fig. 1A), where region 1 is sufficient to support the biological activity of H-rasG12V (11) (Fig. 1C). We can now account for these observations. The FRAP analysis (Fig. 9) showed that GFP-H-rasG12V-Δ2ala, which retains region 1 with the correct spacing from the membrane anchor, displays strong and stable (pure lateral diffusion) membrane association. The FRAP parameters for GFP-H-rasG12V-Δ2ala were very similar to full-length H-rasG12V and were unaffected by cholesterol depletion. Spatial mapping by EM showed that GFP-H-rasG12V-Δ2ala clustered in nonraft microdomains. We conclude that region 1 of the hvr linker provides a major source of affinity for nonraft microdomains. However, this region has to be spaced correctly relative to the membrane anchor to operate efficiently. This is illustrated by GFP-H-rasG12V-Δ2, in which region 1 is not spaced appropriately and functions poorly, resulting in membrane interaction characteristics approaching those of GFP-H-rasG12V-Δhvr: EM and FRAP show that GFP-H-rasG12V-Δ2 is localized to lipid rafts but binds to the membrane with very low affinity (fluorescence recovery is by exchange).

The FRAP studies (Fig. 9) show that the two mutants missing hvr linker region 1 (GFP-H-rasG12V-Δ1 and -Δ1ala) interact stably with the membrane (fluorescence recovery by pure lateral diffusion; Fig. 9A). Deletion of both regions 1 and 2 (GFP-H-rasG12V-Δhvr) results in much weaker membrane association (fluorescence recovery by exchange; Fig. 7A), strongly suggesting that region 2 of the hvr linker (present in H-rasG12V-Δ1 and -Δ1ala) contributes to the association of H-rasG12V with the plasma membrane. The interaction of H-rasG12V-Δ1 and -Δ1ala appears to be with both raft and

nonraft sites, as shown by the EM analysis and FRAP studies following cholesterol depletion. The EM analysis (Fig. 3 and 4) shows that both GFP-H-rasG12V-Δ1 and GFP-H-rasG12V-Δ1ala reside in part in cholesterol-sensitive clusters, colocalized with the raft-resident GFP-tH. Accordingly, the FRAP studies demonstrate that cholesterol depletion weakens but does not abolish the membrane interactions of GFP-H-rasG12V-Δ1 and GFP- H-rasG12V-Δ1ala, resulting in a shift of their fluorescence recovery to exchange (Fig. 9B).

All of the data presented here can be synthesized into a relatively simple model in which three separable forces operate on H-ras at the plasma membrane (Fig. 10). The model illustrates that a repulsive force of the N-terminal domain of H-ras operating primarily against an attractive force from the lipid anchor for lipid rafts is essential for allowing H-ras to exit from lipid rafts. A second attractive force provided by the hvr linker shifts H-ras to nonraft microdomains. Since the repulsive force is greater when H-ras is GTP loaded, the shift to nonraft domains is greater when H-ras is activated. The force from the hvr linker can be resolved further into contributions from regions 1 and 2 of the linker domain, with the attraction for nonraft domains arising primarily from region 1. A prediction of this model, that the membrane affinity of GFP-CTH should be greater than that of GFP-tH, is supported by cell fractionation data (Fig. 8).

In summary, we have integrated two independent and quantitative approaches, FRAP beam size analysis and EM spatial mapping, to study H-ras membrane interactions. While the FRAP studies measure the association dynamics of H-ras mutants with the plasma membrane, the EM analysis maps the distribution and clustering of these proteins in specific microdomains. The data sets therefore yield very different parameters of H-ras membrane interactions, and yet it is important to stress that for H-ras proteins stably associated with the membrane, FRAP can also discriminate between raft-associated and nonraft mutants on the basis of the ability of cholesterol depletion to elevate the lateral diffusion rate (14, 24). For all such proteins [H-ras(wt), H-rasG12V, H-rasG12V-Δ2ala, GFP-tH, and GFP-CTH], the FRAP results are in complete agreement with the EM mapping data, providing a live-cell correlate to the EM studies.

Together, our studies demonstrate that the interactions that regulate H-ras membrane affinity also determine the preference for raft or nonraft microdomains. The combined approach has allowed us to characterize the roles of specific regions of H-ras in its interactions with the membrane. Notably, our findings demonstrate for the first time that three separate regions of H-ras have specific contributions to its affinity to the plasma membrane. The concept that the GDP/GTP loading state not only affects H-ras microlocalization in raft and nonraft domains but also modulates its affinity to the plasma membrane has important implications for H-ras signaling, since Ras association with the plasma membrane is necessary for its biological function (7). In addition, the finding that cholesterol depletion has simultaneous effects on both the lateral segregation and the membrane attachment of H-ras mutants raises the intriguing possibility that the free energy of H-ras lateral segregation is comparable to that of the hydrophobic interaction mediated by the H-ras membrane anchor.

Finally, it is tempting to speculate that the findings presented here have broad implications for other signaling proteins that are lipid anchored to the inner surface of the plasma membrane. For example, it is generally assumed that lipid modifications alone are sufficient for lipid raft association but, as shown here, the microlocalization of a lipid modified protein can also depend on additional structural features of the protein. Furthermore it is possible that other signaling proteins, including the Src kinases, could dynamically regulate their interactions with lipid rafts by a similar mechanism to that described here for H-ras: namely, by generating a repulsive force, modulated by conformational changes in the catalytic domain, to act against the lipid anchor.

## ACKNOWLEDGMENTS

This work was supported by grants from the National Institutes of Health (GM-066717) and the National Health and Medical Research Council to J.F.H. and R.G.P. I.A.P. is a Royal Society University Research Fellow. Y.I.H. is an incumbent of the Zalman Weinberg Chair in Cell Biology.

## REFERENCES

1. **Anderson, R., and K. Jacobson.** 2002. A role for lipid shells in targeting proteins to caveolae, rafts and other lipid domains. Science **296:**1821–1825.
2. **Axelrod, D., D. E. Koppel, J. Schlessinger, E. L. Elson, and W. W. Webb.** 1976. Mobility measurement by analysis of fluorescence photobleaching recovery kinetics. Biophys. J. **16:**1055–1069.
3. **Dietrich, C., B. Yang, T. Fujiwara, A. Kusumi, and K. Jacobson.** 2002. Relationship of lipid rafts to transient confinement zones detected by single particle tracking. Biophys. J. **82:**274–284.
4. **Ehrlich, M., A. Shmuely, and Y. I. Henis.** 2001. A single internalization signal from the di-leucine family is critical for constitutive endocytosis of the type II TGF-beta receptor. J. Cell Sci. **114:**1777–1786.
5. **Elson, E. L., and J. R. Reidler.** 1979. Analysis of cell surface interactions by measurements of lateral mobility. J. Supramol. Struct. **12:**481–489.
6. **Fujiwara, T., K. Ritchie, H. Murakoshi, K. Jacobson, and A. Kusumi.** 2002. Phospholipids undergo hop diffusion in compartmentalized cell membrane. J. Cell Biol. **157:**1071–1081.
7. **Hancock, J. F.** 2003. Ras proteins: different signals from different locations. Nat. Rev. Mol. Cell Biol. **4:**373–384.
8. **Harder, T., P. Scheiffele, P. Verkade, and K. Simons.** 1998. Lipid domain structure of the plasma membrane revealed by patching of membrane components. J. Cell Biol. **141:**929–942.
9. **Hua, X., J. Sakai, M. S. Brown, and J. L. Goldstein.** 1996. Regulated cleavage of sterol regulatory element binding proteins requires sequences on both sides of the endoplasmic reticulum membrane. J. Biol. Chem. **271:** 10379–10384.
10. **Illenberger, D., C. Walliser, J. Strobel, O. Gutman, H. Niv, V. Gaidzik, Y. Kloog, P. Gierschik, and Y. I. Henis.** 2003. Rac2 regulation of phospholipase C-$\beta_2$ activity and mode of membrane interactions in intact cells. J. Biol. Chem. **278:**8645–8652.
11. **Jaumot, M., J. Yan, J. Clyde-Smith, J. Sluimer, and J. F. Hancock.** 2002. The linker domain of the Ha-ras hypervariable region regulates interactions with exchange factors, Raf-1 and phosphoinositide 3-kinase. J. Biol. Chem. **277:** 272–278.
12. **Munro, S.** 2003. Lipid rafts. Elusive or illusive? Cell **115:**377–388.
13. **Niv, H., O. Gutman, Y. I. Henis, and Y. Kloog.** 1999. Membrane interactions of a constitutively active GFP-Ki-Ras 4B and their role in signaling: evidence from lateral mobility studies. J. Biol. Chem. **274:**1606–1613.
14. **Niv, H., O. Gutman, Y. Kloog, and Y. I. Henis.** 2002. Activated K-Ras and H-Ras display different interactions with saturable nonraft sites at the surface of live cells. J. Cell Biol. **157:**865–872.
15. **Petersen, N. O., S. Felder, and E. L. Elson.** 1986. Measurement of lateral diffusion by fluorescence photobleaching recovery, p. 24.21–24.23. *In* D. M. Weir, L. A. Herzenberg, C. C. Blackwell, and L. A. Herzenberg (ed.), Handbook of experimental immunology. Blackwell Scientific Publications, Edinburgh, United Kingdom.
16. **Pralle, A., P. Keller, E. Florin, K. Simons, and J. Horber.** 2000. Sphingolipid-cholesterol rafts diffuse as small entities in the plasma membrane of mammalian cells. J. Cell Biol. **148:**997–1008.
17. **Prior, I. A., A. Harding, J. Yan, J. Sluimer, R. G. Parton, and J. F. Hancock.** 2001. GTP-dependent segregation of H-ras from lipid rafts is required for biological activity. Nat. Cell Biol. **3:**368–375.
18. **Prior, I. A., C. Muncke, R. G. Parton, and J. F. Hancock.** 2003. Direct visualization of Ras proteins in spatially distinct cell surface microdomains. J. Cell Biol. **160:**165–170.

19. **Prior, I. A., R. G. Parton, and J. F. Hancock.** 2003. Observing cell surface signaling domains using electron microscopy. Sci. STKE **2003:**L9.
20. **Ripley, B. D.** 1979. Tests of randomness for spatial point patterns. J. R. Statist. Soc. B **41:**368–374.
21. **Roy, S., R. Luetterforst, A. Harding, A. Apolloni, M. Etheridge, E. Stang, B. Rolls, J. F. Hancock, and R. G. Parton.** 1999. Dominant-negative caveolin inhibits H-Ras function by disrupting cholesterol-rich plasma membrane domains. Nat. Cell Biol. **1:**98–105.
22. **Schutz, G., G. Kada, V. Pastushenko, and H. Schindler.** 2000. Properties of lipid microdomains in a muscle cell membrane visualized by single molecule microscopy. EMBO J. **19:**892–901.
23. **Sharma, P., R. Varma, R. Sarasij, Ira, K. Gousset, G. Krishnamoorthy, M. Rao, and S. Mayor.** 2004. Nanoscale organization of multiple GPI-anchored proteins in living cell membranes. Cell **116:**577–589.
24. **Shvartsman, D. E., M. Kotler, R. D. Tall, M. G. Roth, and Y. I. Henis.** 2003. Differently anchored influenza hemagglutinin mutants display distinct interaction dynamics with mutual rafts. J. Cell Biol. **163:**879–888.
25. **Simons, K., and D. Toomre.** 2000. Lipid rafts and signal transduction. Nat. Rev. Mol. Cell Biol. **1:**31–39.
26. **Slot, J. W., and H. J. Geuze.** 1985. A new method of preparing gold probes for multiple-labelling cytochemistry. Eur. J. Cell Biol. **38:**87–93.
27. **Symons, M.** 1996. Rho family GTPases: the cytoskeleton and beyond. Trends Biochem. Sci. **21:**178–181.
28. **Varma, R., and S. Mayor.** 1998. GPI-anchored proteins are organized in submicron domains at the cell surface. Nature **394:**798–801.
29. **Zacharias, D., J. Violin, A. Newton, and R. Tsien.** 2002. Partitioning of lipid-modified GFPs into membrane microdomains of live cells. Science **296:**913–916.